Supporting Information

Narrowing of Protein NMR Spectral Lines Broadened by Chemical Exchange

Ying Li and Arthur G. Palmer III
Department of Biochemistry and Molecular Biophysics, Columbia University,
New York, New York 10032

1. Numerical optimization to minimize effects of RF inhomogeneity

The optimization was performed with SPINEVOLUTION[1] using a grid search. B_1 inhomogeneity was represented by a Gaussian function with a full-width-at-half-height of 10%. 100 points were sampled from the Gaussian distribution.

1.1 Search for optimal pulse flip angles

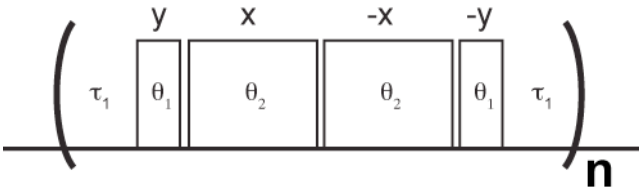

Figure S1 Diagram of the RF cycle with the optimization parameters indicated.

As the first step, a three-parameter optimization was performed to identify the optimal flip angles for the two pairs of outer and inner pulses. The three parameters are θ_1, θ_2 and τ_1/τ_{90}, where θ_1 and θ_2 are the flip angles of the two outer and inner pulses, respectively, as indicated in Figure S1, and τ_{90} is the 90° pulse length. Ratios of pulse lengths or delays are chosen as optimization parameters to ensure that the optimal values are independent of B_1 field. Each pair of outer or inner pulses is of the same length to ensure that the four pulses generate a zero net rotation. Pulse flip angles are varied by changing pulse lengths. Magnetization decay rates calculated at 10 offsets evenly distributed in the range of $-0.5\omega_1$ to 0 are summed up to represent the overall effects of RF inhomogeneity. Only negative offsets are used for calculation because the effects are symmetrical with respect to the zero offset. The starting magnetization is set to be perpendicular to the effective field at the beginning of chemical shift scaling (CSS) period and the magnetization on the plane perpendicular to the effective field is observed. The scaling factor and the orientation of the effective field at zero offset can be determined from the leading term of the effective Hamiltonian

$$H_{eff}^{L} = (\sigma_x I_x + \sigma_y I_y + \sigma_z I_z)\Omega \qquad \text{(S1)}$$

where

$$\sigma_x = -\frac{4\tau_{90}\sin\frac{\theta_1}{2}\left(\sin\frac{\theta_1}{2} + \cos\frac{\theta_1}{2}\sin\theta_2\right)}{\pi\tau_1 + 2(\theta_1 + \theta_2)\tau_{90}} \qquad \text{(S2)}$$

$$\sigma_y = \frac{4\tau_{90}\sin^2\frac{\theta_2}{2}}{\pi\tau_1 + 2(\theta_1 + \theta_2)\tau_{90}} \qquad \text{(S3)}$$

$$\sigma_z = \frac{\pi\tau_1 + 2\tau_{90}\sin\theta_1 + 2\tau_{90}\cos\theta_1\sin\theta_2}{\pi\tau_1 + 2(\theta_1+\theta_2)\tau_{90}} \quad \text{(S4)}$$

Ω is the resonance offset. The scaling factor σ is given by $\sigma = \sqrt{\sigma_x^2 + \sigma_y^2 + \sigma_z^2}$

The results of the optimization indicate that the optimal flip angles do not strongly depend on τ_1/τ_{90} when τ_1/τ_{90} are in the range of 0.7 to 3.4. The optimal values are approximately 90° for θ_1 and 300° for θ_2. When $\tau_1/\tau_{90} < 0.7$, the ratio of θ_2 to θ_1 is still very close to 3.0 though θ_1 is much larger than 90°. When $\tau_1/\tau_{90} > 3.4$, the optimal values for flip angles cannot be found. Figure S2 shows the line broadening by RF inhomogeneity as a function of two pulse flip angles when $\tau_1/\tau_{90} = 1$ (Figure S2A) and $\tau_1/\tau_{90} = 2$ (Figure S2B), respectively. Optimal parameters that generate scaling factors ranging from 0.2 to 0.5, as well as the corresponding orientation of the effective field are included in Table S1.

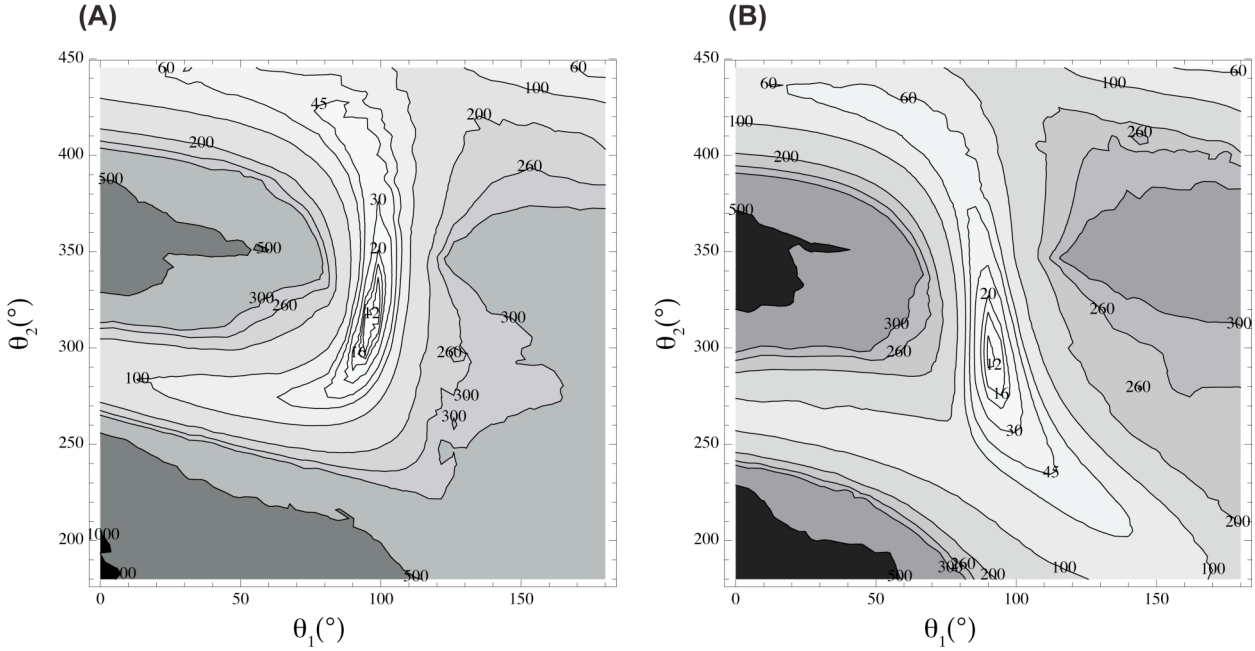

Figure S2 Contour plots of the line broadening by RF inhomogeneity as a function of two pulse flip angles, θ_1 and θ_2 when (A) $\tau_1/\tau_{90} = 1.0$ and (B) $\tau_1/\tau_{90} = 2.0$. The contour levels represent the sum of magnetization decay rates calculated for 10 offsets in the range of $-0.5\omega_1$ to 0.

Table S1 Optimal parameters for scaling factors ranging from 0.2 to 0.5 and the corresponding orientations of effective field

σ	θ_1(°)	θ_2(°)	τ_1/τ_{90}	unit vector representing the orientation of B_{eff}
0.218	139.5	346.5	0.1	(-0.853, 0.015, 0.522)
0.252	108	319.5	0.5	(-0.333, 0.128, 0.934)
0.292	99	324	0.9	(-0.224, 0.089, 0.971)
0.339	94.5	306	1.2	(-0.091, 0.174, 0.981)
0.408	90	297	1.8	(-0.028, 0.198, 0.980)
0.450	90	292.5	2.2	(-0.017, 0.206, 0.979)
0.497	94.5	283.5	2.6	(0.021, 0.234, 0.972)

1.2 Search for optimal delays with fixed pulse flip angles

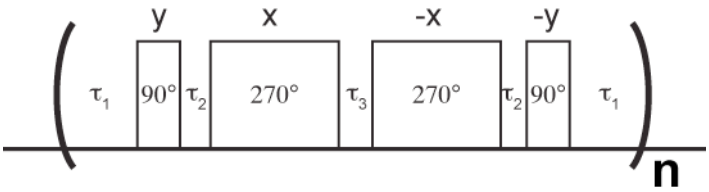

Figure S3 Diagram of the RF cycle with the optimization parameters indicated.

When the pulse sequence is implemented on the spectrometer, short delays between pulses must be inserted to allow phase switching. In the second step of optimization, we inserted delays between pulses as shown in Figure S3. We chose to optimize three variables, τ_1/τ_{90}, τ_2/τ_{90} and τ_3/τ_{90} when pulse flip angles θ_1 and θ_2 were kept at 90° and 270°, respectively. These two values were chosen to generate an effective B_1 field with a zero x-component when $\tau_2 = 0$. The scaling factor and the orientation of the effective field at zero offset can be determined from the leading term of the effective Hamiltonian

$$H_{eff}^{L} = (\sigma_x I_x + \sigma_y I_y + \sigma_z I_z)\Omega \quad \text{(S5)}$$

where

$$\sigma_x = -\frac{2\tau_2}{8\tau_{90} + 2\tau_1 + 2\tau_2 + \tau_3} \quad \text{(S6)}$$

$$\sigma_y = \frac{4\tau_{90} - \pi\tau_3}{\pi(8\tau_{90} + 2\tau_1 + 2\tau_2 + \tau_3)} \quad \text{(S7)}$$

$$\sigma_z = \frac{4\tau_{90} + 2\pi\tau_1}{\pi(8\tau_{90} + 2\tau_1 + 2\tau_2 + \tau_3)} \quad \text{(S8)}$$

The scaling factor σ is given by $\sigma = \sqrt{\sigma_x^2 + \sigma_y^2 + \sigma_z^2}$

We found that τ_2 is small for all optimal solutions and Figure S4 shows the line broadening as a function of τ_1/τ_{90} and τ_3/τ_{90}, when $\tau_2 = 0.03\ \tau_{90}$, which corresponds to 3 μs when τ_{90} = 100 μs. The quality of the optimal solution is comparable to that obtained from using optimal flip angles without inserting delays between pulses. However, using the flip angles of 90° and 270° has the advantage of generating an effective field that does not have an x-component.

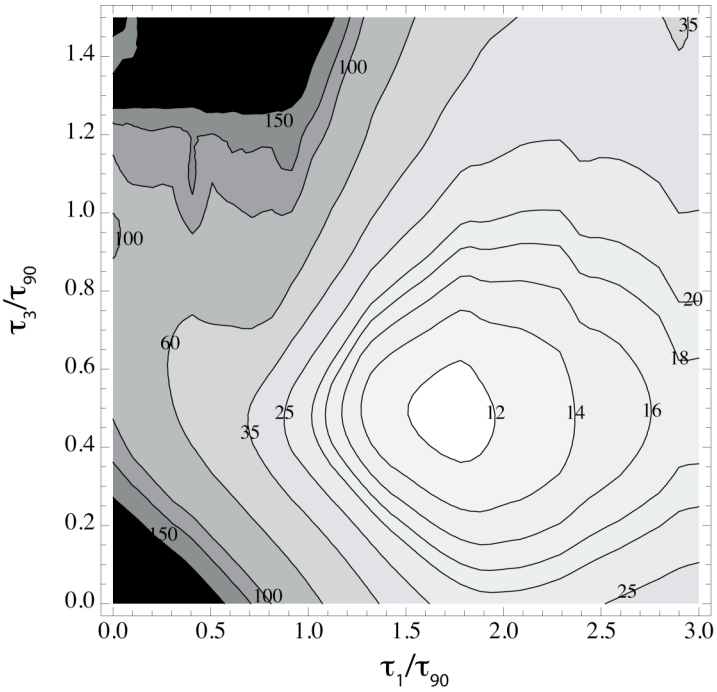

Figure S4 Contour plot of the line broadening by RF inhomogeneity as a function of τ_1/τ_{90} and τ_3/τ_{90} when $\tau_2 = 0.03\ \tau_1$. The contour levels represent the sum of magnetization decay rates calculated for 10 offsets in the range of $-0.5\omega_1$ to 0.

2. Additional experimental details for experiments described in the main text

For CSS experiments, in general, the orientation of the effective field is not along z-axis and when it deviates significantly from z-axis, an extra pulse after the CSS period is needed to rotate the magnetization to the transverse plane for detection. The starting magnetization also must be perpendicular to the effective field to avoid zero frequency artifacts. For easy implementation, the parameters chosen for all experiments result in effective fields that are nearly parallel to z-axis (less than 8° deviation) and do not have an x-component. The starting magnetization therefore can be easily set to be along x-axis.

The RNase A sample used for TROSY experiments contains 0.78 mM protein in a buffer containing 5 mM 2-(N-morpholino)ethanesulfonic acid (MES) at pH 6.4 and 7 mM NaCl. For the TROSY experiment with CSS, constant sample heating was maintained for each t_1 increment by incorporating appropriate number of pulses during the inter-scan delay. The normal TROSY experiment also contains such pulses to maintain the same heating as in the TROSY with CSS.

3. Experiments on ubiquitin to verify that the four-pulse scheme offers good compensation to RF inhomogeneity

To confirm that good compensation to RF inhomogeneity is achieved using the four pulse scheme with the set of parameters selected for experiments on RNase A as described in the main text, we performed the same TROSY experiment with CSS ($\sigma = 0.42$) on a sample of ^{2}H, ^{15}N-labelled ubiquitin, which do not have resonances significantly broadened by chemical exchange. Figure S5 shows the ratio of the line widths measured from the TROSY experiments with and

without CSS as a function of resonance offsets. The ratios do not show obvious dependence on offsets, indicating that the scheme together with the selected set of optimal parameters compensates RF inhomogeneity adequately. The average ^{15}N line width is 5.3 Hz for the normal TROSY and 7.0 Hz for the TROSY with CSS.

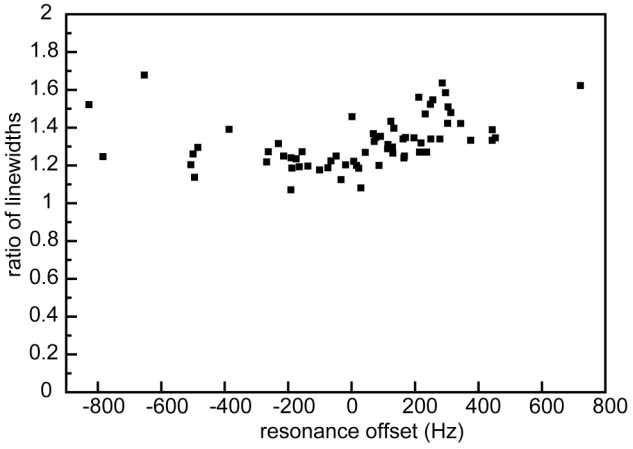

Figure S5 The ratio of ^{15}N line widths measured from ^{15}N-^{1}H TROSY with and without CSS shown as a function of resonance offsets. The data were acquired on a sample of ^{2}H, ^{15}N-labelled ubiquitin at 500 MHz ^{1}H frequency and 293 K.

4. Effective Hamiltonian

An exact expression for the effective Hamiltonian can be obtained by using the exact effective Hamiltonian theory.[2] Under CSS, the effective Hamiltonian has the functional form $H_{eff} = \sigma \Omega \vec{n} I$, where Ω is the resonance offset, σ is the CSS factor, $\vec{n}$ is the unit vector representing the orientation of the effective field.

When series expansion is performed on the effective Hamiltonian, the scaling factor has the functional form $\sigma = \sigma_0 + c_2 r^2 + c_4 r^4 + c_6 r^6 + \ldots$, where $r = \Omega/\omega_1$. The scaling factor depends only on the ratio of resonance offset to B_1 field. Because the RF cycle produces a symmetric Hamiltonian with respect to the center time point in the interaction frame defined by RF pulses, all odd order terms vanish. The optimization parameters have been chosen to maintain this symmetry.

For the set of parameters ($\tau_1 = 2\tau_{90}$, $\tau_2 = 0$, $\tau_3 = 0.5\tau_{90}$) used for experiments on RNase A,
$\sigma = 0.4264 - 0.0776 r^2 + 0.4637 r^4 - 0.9374 r^6 + \ldots$

The coefficient for the 2nd order term is small, consistent with uniform scaling factors across the entire effective bandwidth. Figure S6 shows the dependence of scaling factor and the orientation of effective field on the resonance offsets calculated from the exact expression of effective Hamiltonian. When the absolute value of the offset is smaller than $0.5\omega_1$, the scaling factor is uniform and the z-component of the effective field is nearly 1.0.

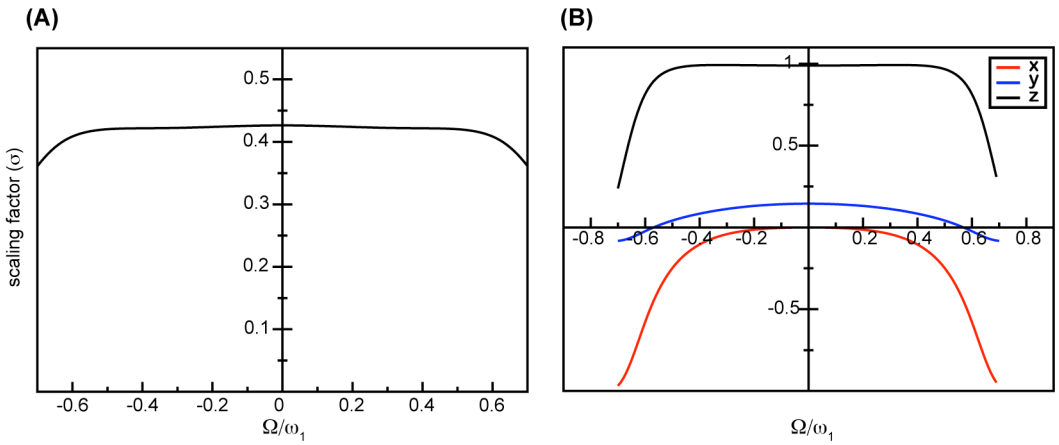

Figure S6 (A) Scaling factor as a function of resonance offset (B) Orientation of the effective field as a function of resonance offset.

5. Effective relaxation rate resulting from averaging longitudinal and transverse relaxation

During each RF cycle, longitudinal and transverse relaxation are averaged and the effective relaxation rate depends on the trajectory of magnetization. In this section, transverse relaxation resulting from chemical exchange is not considered. We have numerically calculated the offset dependence of the effective relaxation rate and the results are shown in Figure S7. The set of parameters ($\tau_1 = 2\tau_{90}$, $\tau_2 = 0$, $\tau_3 = 0.5\tau_{90}$) used for CSS is the same as for the experiment performed on RNase A except that the short delay τ_2 is set to zero for simplicity. For macromolecules, the longitudinal relaxation rate R_1 is much smaller than the transverse relaxation rate R_2 and therefore has been neglected for simplicity. The variation in the effective relaxation rate is very small within the effective bandwidth and is only approximately 3% of R_2. At resonance offsets larger than $0.1\omega_1$, the effective relaxation rate is essentially a constant.

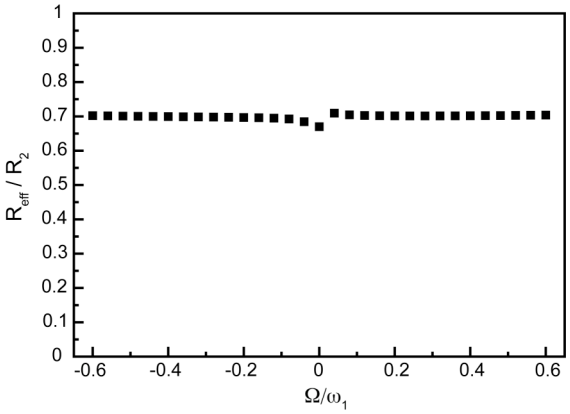

Figure S7 The ratio of effective relaxation rate to R_2 as a function of resonance offset, which is represented as the ratio of offset to B_1 field.

6. Transverse relaxation resulting from chemical exchange in the presence CSS

6.1 Dependence of the line narrowing effects on B_1 field or pulsing rate

Different from relaxation resulting from dipolar coupling and chemical shift anisotropy, transverse relaxation due to chemical exchange does not depend on the trajectory of magnetization if the isotropic chemical shifts are averaged on a time scale much faster than that

of the chemical exchange process. Under this condition, the only factor that determines the relaxation rate is the scaling factor σ for a given chemical exchange process. We have compared the dependence of R_{ex} on the B_1 field strength of soft pulses or pulsing rate of hard pulses when the four-pulse scheme and the divided-evolution scheme are applied for CSS. Figure S8 shows an example of numerically calculated relaxation rates under CSS using a particular set of parameters for the chemical exchange process ($p_A = 0.95$, $p_B = 0.05$, $k_{ex} = 1500\ s^{-1}$, $\Delta\omega = 1500\ s^{-1}$). A scaling factor of 0.43 is used for both schemes, which is the same as that used for experiments on RNase A. For the four-pulse scheme, the flip angles are fixed and pulse lengths and delays are adjusted according to the B_1 field. For the divided-evolution scheme, the 90° pulse length of hard pulses is 40 μs and 8 π pulses with XY8 phase cycle are applied in each RF cycle. It is evident that the four-pulse scheme based on soft pulses allows the relaxation rate to approach its minimal value (for a given scaling factor) faster when the B_1 field or the pulsing rate increases.

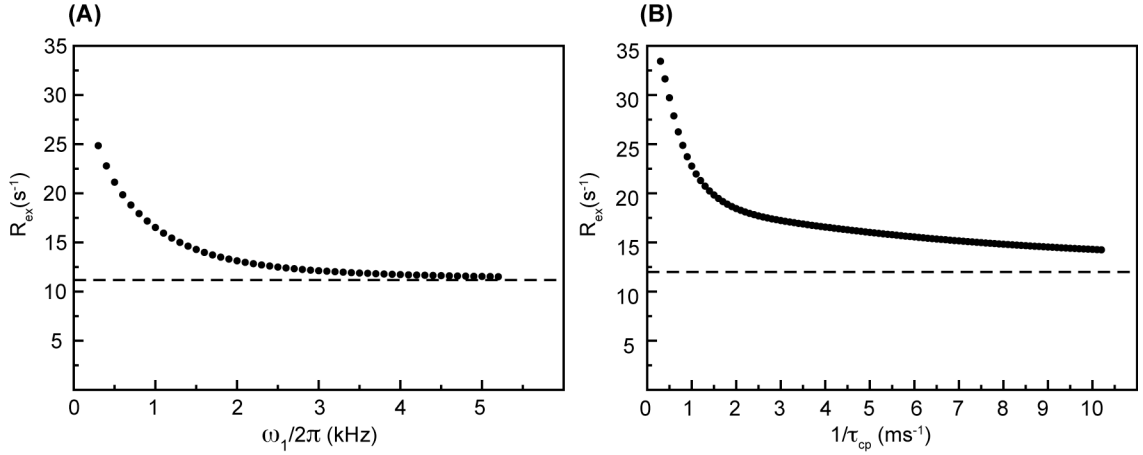

Figure S8 Transverse relaxation rate as a function of either B_1 field or pulsing rate when CSS is performed with (A) the four-pulse scheme described in this work and (B) divided evolution. τ_{cp} is the spacing between hard pulses. The dashed lines represent the relaxation rates when either $\omega_1/2\pi$ or $1/\tau_{cp}$ approaches infinity.

6.2 Dependence of line narrowing effects on chemical exchange parameters when the B_1 field is sufficiently strong

A previous theoretical study[3] has shown that transverse relaxation rate is scaled by σ^2 if the chemical exchange is in the fast exchange regime on the chemical shift time scale and the RF pulses are infinitely strong. Although different RF pulse schemes were used for CSS in this theoretical study, our results from numerical calculations using the four-pulse scheme presented in this work completely agree with the conclusion. The conclusion is also supported by our data on DMTCA as presented in Figure 1 of the main text.

When the chemical exchange process is outside the fast exchange limit, the relationship between transverse relaxation rate and the CSS factor σ is complicated. Figure S9 shows the numerically calculated ratio of transverse relaxation rates of the major species with and without CSS as a function of $\Delta\omega/k_{ex}$. The calculations used the four-pulse scheme described in this work and a

two-site exchange mode. When the chemical exchange process is in the intermediate-to-slow exchange regimes, the transverse relaxation is scaled by a factor larger than σ^2 .

When the chemical exchange process is in the slow exchange limit, the CSS method is no longer applicable. In this regime, the transverse relaxation rate is not sensitive to the difference in the chemical shifts of exchanging species, and therefore CSS does not change the transverse relaxation rate.

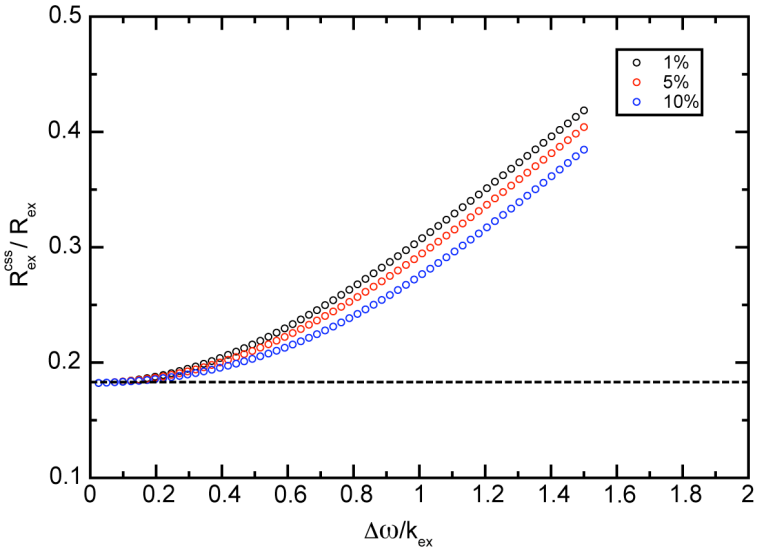

Figure S9 Ratio of transverse relaxation rates with and without CSS as a function of $\Delta\omega/k_{ex}$. The rate constant of the exchange process is fixed at 1500 s^{-1} and the B_1 field is fixed at 10 kHz, which is much larger than the rate constant. Other parameters including fractional populations and the differences in chemical shifts of the exchanging species are varied. A two-site exchange model is employed for the calculation. The fractional population of the minor species is indicated in the legend. The dashed line indicates the limiting value σ^2, where $\sigma = 0.43$.

References:

(1) Veshtort, M.; Griffin, R. G. *J. Magn. Reson.* **2006**, *178*, 248-282.
(2) Untidt, T. S.; Nielsen, N. C. *Phys. Rev. E* **2002**, *65*, 021108.
(3) Vega, A. J.; English, A. D.; Mahler, W. *J. Magn. Reson.* **1980**, *37*, 107-128.